DOI:
10.1148/radiol.220122

Document Version
Peer reviewed version

Multi-Ethnic Study of Atherosclerosis: Relationships between LV Shape from Cine MR Imaging and 10-year Outcomes

Charlène A. Mauger[a,b*] Ph.D., Kathleen Gilbert[b*] Ph.D., Avan Suinesiaputra[c] Ph.D., David A. Bluemke[d] MD PhD MsB, Colin O. Wu[e] , Joao A.C. Lima[e] M.D., Alistair A. Young[c] Ph.D., Bharath Ambale-Venkatesh[e] Ph.D.

[a] *Department of Anatomy and Medical Imaging, Faculty of Medical and Health Sciences, University of Auckland, 85 park road, Grafton, Auckland, 1023, New Zealand*

[b] *Auckland Bioengineering Institute, University of Auckland, 70 Symonds street, Auckland, 1010, New Zealand*

[c] *Department of Biomedical Engineering, King's College London, UK*

[d] *Department of Radiology, University of Wisconsin School of Medicine and Public Health, Wisconsin, USA*

[e] *Department of Cardiology, Johns Hopkins Medical Center, Baltimore, USA*

*Contributed equally

Corresponding author

Dr Charlene A. Mauger,
Email: c.mauger@auckland.ac.nz
Address: Department of Anatomy and Medical Imaging, Faculty of Medical and Health Sciences, University of Auckland, 85 park road, Grafton, Auckland, 1023, New Zealand
Phone: +64 21 251 8911

Funding

This work was funded by the Health Research Council of New Zealand (17/234). We also acknowledge the support of NVIDIA Corporation with the donation of the Titan X Pascal GPU used for this research. MESA and the MESA SHARe project are conducted and supported by the National Heart, Lung, and Blood Institute (NHLBI) in collaboration with MESA investigators. Support for MESA is provided by contracts 75N92020D00001, HHSN268201500003I, N01-HC-95159, 75N92020D00005, N01-HC-95160, 75N92020D00002, N01-HC-95161, 75N92020D00003, N01-HC-95162, 75N92020D00006, N01-HC-95163, 75N92020D00004, N01-HC-95164, 75N92020D00007, N01-HC-95165, N01-HC-95166, N01-HC-95167, N01-HC-95168 and N01-HC-95169 from the NHLBI, and by grants UL1-TR-000040, UL1-TR-001079, and UL1-TR-001420 from the National Center for Advancing Translational Sciences (NCATS). The authors thank the other investigators, the staff, and the participants of the MESA study for their valuable contributions. A full list of participating MESA investigators and institutions can be found at http://www.mesa-nhlbi.org.

Manuscript type: Original Research

Data sharing statement: Data analyzed during the study were provided by a third party. Requests for data should be directed to the provider indicated in the Funding.

Article type: Original Research

Summary: CMR-derived LV event-specific remodeling signatures provide quantitative information on sub-clinical disease and were more predictive of 10-year cardiovascular events than standard mass and volumes after adjustment for cardiovascular risk factors.

Key results:

- In a retrospective study of 4,618 participants of MESA, event-specific remodeling signatures computed from 3D MRI shape analysis improved prediction of 10-year events in heart failure, coronary heart disease, and all cardiovascular disease events.
- Participants with high-risk heart failure scores had a 10-year survival of 56% compared with 95% for low-risk scores.
- Personalized remodeling signatures can be used to automatically score LV remodeling associated with adverse events with respect to a reference cohort.

Abbreviations and Acronyms

CACS = Coronary artery calcium score

CHD = coronary heart disease

CVD = cardiovascular disease

EDV(i) = (indexed) end-diastolic volume

EF = ejection fraction

ESV(i) = (indexed) end-systolic volume

HF = heart failure

IPA = index of prediction accuracy

M(i) = (indexed) mass

RS = remodeling signature

PLS = partial least squares

Abstract

Background: Left ventricular (LV) subclinical remodeling is associated with adverse outcomes and indicates mechanisms of disease development. Standard metrics such as LV mass and volume may not capture the full range of remodeling.

Purpose: To quantify relationships between LV 3D shape and incident cardiovascular events over 10-years.

Materials and Methods: 5,098 participants from the Multi-Ethnic Study of Atherosclerosis population, free of clinical cardiovascular disease, underwent cardiac magnetic resonance imaging in 2000-2002. LV shape models were automatically generated using a machine learning workflow. Event-specific remodeling signatures (RS) were computed using partial least squares regression, and random survival forests were used to determine which features were most associated with incident of heart failure (HF), coronary heart disease (CHD), and all cardiovascular events (CVD) over a 10-year follow-up period. The discrimination improvement of adding LV shape to traditional cardiovascular risk factors, coronary calcium score and NT-proBNP was assessed using the index of prediction accuracy and the time-dependent area under the receiver operating characteristic curve (AUC). Kaplan-Meier survival curves were used to illustrate the abilities of RS to predict the endpoints.

Results: 4,618 participants had sufficient 3D information to generate patient-specific LV models (age 60.6±9.9 years, 55% women). 147 HF, 317 CHD and 455 CVD events were observed. The addition of LV RS to traditional cardiovascular risk factors improved the 10-year AUC for prediction and achieved better performance than LV mass and volumes: HF (AUC: 0.83±0.01 and 0.81±0.01 respectively, $p<0.05$), CHD (0.77±0.7 and 0.75±01 respectively, $p<0.05$) and CVD (0.75±0.0 and 0.74±0.0 respectively, $p<0.05$). Kaplan-Meier

analysis demonstrated participants with high-risk HF RS had a 10-year survival of 56% compared with 95% for low-risk scores.

Conclusions: LV event-specific RS were more predictive of 10-year HF, CHD and CVD than standard mass and volume, and enable an automatic precision medicine approach to tracking remodeling.

Introduction

Left ventricular (LV) mass and volumes have been identified as important metrics of remodeling in patients with myocardial infarction and heart failure (HF) (1,2). LV subclinical remodeling may also occur in asymptomatic individuals prior to the establishment of clinical symptoms in response to exposure to cardiovascular risk factors. In asymptomatic population-based studies, LV end-systolic (ESV) and end-diastolic (EDV) volumes and chamber diameters, as well as relative wall thickness and indexed LV mass (LVMi), have been shown to be predictive of HF (3,4). In the Framingham Heart Study (5), larger LV chamber dimension, lower systolic dimension changes (6) and hypertrophy (7) were associated with future adverse events. In the Multi-Ethnic Study of Atherosclerosis (MESA), LV mass and volume were associated with incident coronary heart disease (CHD), as well as HF (8), while LV sphericity was associated with both incident CHD (low sphericity) and HF (high sphericity) (9).

However, current measures of LV mass, volumes and sphericity do not capture all the information available on LV shape. Multidimensional LV shape measures have shown significant relationships with sub-clinical disease and risk factors (10-12) and are more strongly associated with cardiovascular risk factors than traditional mass and volume metrics (10,11,13). Also, machine learning methods such as random survival forest analysis show promise to identify which factors are most strongly related with cardiovascular outcomes (14). A better knowledge of the pre-clinical remodeling patterns associated with adverse incident events would aid understanding of the mechanisms of developing disease.

In this paper, we define event-specific ‘signatures’ of preclinical LV remodeling, expressed as a set of event-specific remodeling scores, which are optimally associated with incident HF, CHD, and all cardiovascular events (CVD) over a 10-year follow-up period in MESA. A machine learning pipeline was used to automatically generate patient-specific shape models

and determine the event-specific shape signatures. We hypothesized that multidimensional shape signatures would be more strongly associated with incident events than standard LV mass, volumes, and ejection fraction (EF) measures.

Materials and Methods

Study Design

MESA is an ongoing prospective multicenter population-based study in the United States designed to examine disease development from pre-clinical manifestations to clinical symptoms (15). 6,814 multi-ethnic men and women free of clinically apparent cardiovascular disease were enrolled between 2000 and 2002. All participants gave informed consent, and the study was approved by the institutional review boards of all MESA centers. Atlas results from 1,991 MESA individuals have been previously reported (10). Also, results of a machine learning atlas generation pipeline using 1,052 MESA individuals was recently reported (16). Here, we report for the first time on relationships between atlas score and cardiovascular outcomes and propose a framework for using shape-atlases in personalized risk prediction and prognostication.

Incident HF, CHD and CVD events as defined in the MESA study were used as endpoints in this study. Criteria for probable HF included symptomatic HF diagnosed by a doctor and treatment, while definite HF also required evidence of one or more other criteria (including pulmonary edema/congestion by chest X-ray, dilated ventricle or poor LV function by echocardiography or ventriculography, or evidence of left ventricular diastolic dysfunction). Criteria for CHD included myocardial infarction, resuscitated cardiac arrest, definite and probable angina, and CHD related death. CVD events included stroke, CHD, atherosclerotic death, stroke death, and CVD death. The event time was defined as elapsed days between

baseline examination and event. More information about event definition and adjudication is given in the Supplementary Materials, and (8).

MRI Protocol

Cardiovascular MRI (CMR) was performed on 1.5T MR scanners at six institutions using Siemens and General Electric. Details of the imaging protocol can be found in (17). Images were acquired in four-chamber, two-chamber long axis and short axis slices with a gradient recalled echo sequence (typical TR of 8-10ms; TE of 3-5ms, flip angle 20°), field of view 360-400 mm, pixel size from 1.4 to 2.5 mm, and slice thickness of 6mm with 20-30 frames per slice (temporal resolution <50ms).

Event-specific Remodeling Signatures

An automatic end-to-end pipeline described in (16) was used to generate 3D segmentation of the images for quantification of LV shape at end-diastole and end-systole. LV shape models were constructed as described in (10,13). The processing pipeline is described in the Supplementary Materials and illustrated in Figure S1. Partial Least Squares (PLS) decomposition (18) was applied to the 3D patient-specific geometries to extract event-specific remodeling signatures (RS). The RS represent a set of event-specific remodeling variations, expressed as scores. Time-to-event (in days) was used as the response variable and the LV shape models were used as predictors. PLS latent variable scores (as z-scores) were used as the event-specific RS. The number of latent variables was set to 30 and associated scores were labeled RS1, RS2, …, RS30 in order of decreasing correlation between shape and time-to-event.

Relationship of LV Geometry with Events

Three random survival forest (RSF) models (19), M1, M2, and M3, were compared to assess the strength of relationships between LV shape at baseline and endpoints over a 10-year follow-up. M1 used demographics and traditional cardiovascular risk factors only as predictor

variables. These were: age, sex, race, body mass index, height, weight, smoking, systolic blood pressure, anti-hypertensive medication use, diabetes mellitus, fasting glucose, high-density lipoprotein, total cholesterol, resting heart rate, beta-blocker use, and either log(calcium score (CACS) + 1) for CHD and CVD, or log(NT-proBNP) for HF. M2 comprised all M1 predictors plus EF, LVM, ESV and EDV. EDV, ESV and LVM were not adjusted for body surface area as height and weight were also included as predictors in the models and the use of ratios in regression analysis can lead to spurious results (20). M3 comprised M1 predictors plus 30 event-specific RS derived from the PLS analysis. Each model was trained separately for each endpoint. For each RSF model, an initial RSF was built, and variables ranked based on the mean of the minimal depth of the maximal subtree over the entire forest. The lower the depth, the higher the predictive power. The top ranked variables (those with a depth smaller than the mean depth of all the features) were selected for the final RSF and the model performances were evaluated. The dataset was randomly split into 70% training and 30% testing. This operation was repeated five times, similar to a five-fold cross validation, to avoid comparison bias due to training/test data selection.

Statistics

Analyses were carried out in R (21). A p-value <0.05 was considered significant. The discrimination improvement of adding LV shape was assessed using the index of prediction accuracy (IPA) (22) and the time-dependent area under the receiver operating characteristic curve (AUC) for time-to-event outcomes (23).

Time-dependent sensitivity and positive predictive value (PPV) were also extracted from the time-dependent ROC curves. PPV was chosen over specificity due to low event rates. Survival curves were obtained in a Kaplan Meier analysis and log-rank tests were used to compare survival curves between groups.

Results

Population statistics and patient-specific models

Table 1 shows cohort characteristics. From 5,098 participants who underwent MRI examination at baseline, 4,618 participants were used in this study (Figure 1). The median follow-up time was 8.5 years. From the 4,618 participants, 147 (3.1%) had HF, 317 (6.9%) had CHD and 455 (10%) had CVD. Note that one participant could be associated with multiple outcomes. Participants with events were usually older and more likely to be men. Diabetes, smoking, high cholesterol, higher CACS and NT-ProBNP, heart rate, and body weight were also associated with events.

Performance Evaluation

PLS z-scores were used as event-specific RS. Table 2 shows the average IPA at year-10 from the testing datasets across the five-fold cross-validation for each model and each endpoint. For all endpoints, the addition of imaging parameters and proven biomarkers showed improved performance. Inclusion of LV mass and volume increased prediction performance for each endpoint (M2). For all outcomes of interest, M3 performed the best, showing the highest IPA and AUC. The increase in AUC between M2 and M3 was significant for each endpoint ($p<0.05$). The improvement in IPA and AUC suggests that LV shape is more strongly related with subsequent outcomes than LV mass and volumes. Improvement in IPA and AUC was most pronounced in HF (11.9 against 14.6, $p<0.05$) suggesting a stronger relationship between shape and subsequent HF, relative to CVD and CHD (11.8 vs 12.7 and 11 vs 11.5 respectively, $p<0.05$). M3 also achieved the highest time dependent PPV for each endpoint.

Hazard ratios and their 95% intervals from multivariable Cox regression on these parsimonious PLS-based models can be found in Table S1. Proportional Hazard assumption was tested using Schoenfeld residuals and no violations were found.

Relationship between selected predictors and cardiovascular events

Table 3 shows the top six variables selected by the final random survival forest model for the prediction of CHD, HF and CVD. PLS remodeling signatures could be different between the different endpoints but were among the strongest associations for each event. To interpret each RS, Figure 2 shows correlation between top RS and LV indexed mass and volumes, sphericity, conicity, relative wall thickness, mass-to-volume ratio (LVM/EDV), stroke volume (EDV-ESV), EF ((EDV-ESV)/EDV) and longitudinal shortening (LS). Calculation of these clinical indices is shown in Figure S2. Figure 3 shows PLS RS for each endpoint (top panel) and the association between LV shape and survival probability is visualized using partial dependence plots (bottom panel), showing how each variable (predictor) affected the model's predictions. Kaplan-Meier survival curves (middle panel) are used to illustrate the abilities of remodeling scores to predict the endpoints. Partial dependence plots for the top three cardiovascular risk factors (non-RS) for each event class are provided in Figure S3.

For incident HF, eight variables were selected by the random survival forest, including: age, fasting glucose, NT-proBNP, systolic blood pressure and heart rate and three PLS RS. The first remodeling signature (RS1) had the strongest correlation between shape and outcome and was associated with lower systolic function, shown by reduced EF and longitudinal shortening (Figure 2 and Figure 3) with increasing risk. The first pattern was also characterized by an increase in LVM and LV volumes but no change in relative wall thickness, in accordance with an eccentric hypertrophy at higher risk. The second remodeling signature (RS2) was associated with reduced LV volume and longitudinal shortening with higher risk. RS3 was associated with increased sphericities, mass-to-volume

ratio, and relative wall thickness with constant LVMi, with higher risk. This suggests that concentric hypertrophy with normal EF and reduced longitudinal systolic function at baseline was also associated with incident HF. The existence of these two types of remodeling associated with HF suggests heterogeneous disease mechanisms. Figure 3 shows that the 10-year survival of high-risk scores was 56%, compared with 95% for low-risk scores.

For incident CHD, seven variables were selected: age, systolic blood pressure, smoking, high-density lipoprotein level, positive CACS and two PLS remodeling signatures (RS1 and RS2). CACS was by far the most important. RS1 was associated with an increase in conicity and a decrease in sphericity at higher risk (Figure 2 and Figure 3). This mode was also associated with LV hypertrophy (increase in mass-to-volume ratio, relative wall thickness and decrease in volumes), typical of concentric geometry, as well as a decrease in longitudinal shortening and an increase in EF at higher risk. RS2 was characterized by both a decrease in LV function and a concomitant increase in LV dimension with a slight/negligible increase in relative wall thickness, consistent with eccentric hypertrophy at higher risk.

Incident CVD was associated with 15 variables: positive CACS, age, fasting glucose, heart rate, high-density lipoprotein level, systolic blood pressure and nine PLS modes. Age, systolic blood pressure and presence of CACS were among the top predictors among risk factors for incident CVD. As for CHD, the first two most important shape predictors were associated with concentric remodeling and eccentric hypertrophy respectively. The third shape predictor (RS3) was characterized by an increase in sphericity and apical conicity at both ED and ES at higher risk.

Figure 4 summarizes each RS in terms of currently understood remodeling patterns. For incident HF, three patterns were identified (Figure 4): (i) an eccentric hypertrophy with reduced systolic function (RS1), (ii) a concentric remodeling with increased sphericity,

reduced LS but with preserved EF (RS2), and iii) increased conicity associated with apical dilation (RS3). The RS1 signatures for incident CHD and CVD were both associated with concentric hypertrophy as in (24), with somewhat increased EF and reduced longitudinal shortening, likely associated with elevated systolic blood pressure and increased torsion (31). RS2 for both CHD and CVD was associated with decreased LS in agreement with (34,35).

The global remodelling signatures were also associated with local functional changes. Supplementary Figure S4 illustrates different regional wall thickening patterns captured by HF RS1 vs CHD RS1. For example, HF RS1 was associated with reduced infero-septal wall thickening, whereas CHD RS1 was associated with increased mid-ventricular wall thickening and somewhat reduced apical radial thickening, consistent with compensated LV remodeling (32,33).

Discussion

Although LV mass, volumes and sphericity are known to be associated with adverse events in clinical and sub-clinical disease, broader relationships between LV shape and developing disease are still poorly understood. In this study, we identified LV remodeling signatures associated with incident HF, CHD, and CVD over a 10-year follow-up period in an asymptomatic population. We then used survival modeling in the context of shape analysis to investigate RS indicative of disease mechanisms. Shape signatures offer new analysis tools which are more powerful than traditional mass and volume measures. This enables a method for capturing fine-grain imaging features that results in additional prognostic power and provides additional knowledge of complex remodeling. In addition, we provided associations of LV geometry with cardiovascular events and we showed how patient-specific

RS scores related to each endpoint and incorporated several heterogenous aspects of remodeling. This confirms findings in (24,25) suggesting that measurements of LV geometry carry useful information over and above that conferred by mass, volume, and EF alone.

Automatic computation of patient-specific RS scores for each event class enables prospective studies to be conducted to evaluate the effects of treatment on the z-scores over time. Shape changes associated with changes in z-scores can be visualized and related to other factors such as exercise tolerance or other biomarkers. Analogous to polygenic risk scores, which have been shown to be predictive of HF events independently of risk factors (26), event-specific RS scores enable high-dimensional shape features to be distilled to a few scores, with the added benefit that treatment effects can be automatically evaluated. Patient-specific scores can then be evaluated in terms of disease progression in a precision medicine framework by tracking the amount of RS present in each patient.

Unlike many other machine learning algorithms, the computed RS can be visualized and interrogated for specific physiological mechanisms of disease development. The links between these patterns and microstructural and genetic pathways (27,28) can be investigated by analysis of the RS z-scores. Although some information may be captured by mass, volumes and ejection fraction, the significantly higher discrimination observed for M3 vs M2 indicates that additional prognostic information is present in the RS. This was higher than the improvement shown between M1 and M2, showing that shape information is prognostically more powerful than standard mass/volume metrics.

Our results support the finding that both eccentric and concentric hypertrophy are associated with incident HF but with a different magnitude of risk (Figure 3a), in accordance with (4). RS1 may be linked with increased wall stress (Laplace law) whereas RS2 is linked with reduced longitudinal systolic function with preserved EF in agreement with previous studies (29,30).

The first limitation of our study is the low rate of events. Incident HF represented 3.1%, CHD represented 6.9% and CVD was identified in 10% which may lead to model bias towards event-free participants. The PPVs reported in Table 2 may therefore seem low as the PPVs should range between 0 and 100%. However, as the PPVs are based on prevalence, having a high PPVs with such low event rates would require an AUC >0.95 (95% specificity and 95% sensitivity would give a PPV of 38% for CHF for example). Another limitation of our study is shape bias from the use of gradient recalled echo imaging. Steady-state free precession is now the current standard for CMR and shapes differ between the two protocols (36). With further advances in CMR protocols, transfer learning may be required to adapt the current algorithms. However, previous studies have shown that shape models can be corrected between protocols (36), and atlas analyses are robust to methodology (13). Further validation should be performed on a dataset with a higher rate of events to further improve associations. Validation on an independent population should also be performed to confirm the generalizability of the remodeling signatures. Further study distinguishing between HF with preserved EF and reduced EF should be performed when more participants in each category are available. We have not investigated radiomics features which have been shown to provide prognostic information (37,38). Finally, future work should include description of shape changes in the standard AHA segments, which may aid interpretation of the RS. Note that regional information is captured by the global RS, since information from all points are included in the PLS computation (39).

In conclusion, our study demonstrates that LV shape signatures are independently associated with cardiovascular events over a 10-year follow period in a large asymptomatic population and are of greater prognostic value than traditional mass and volume measures. These personalized remodeling signatures, automatically calculated from standard medical imaging examinations, provide event-specific signatures and unravel unique mechanistic information on the development of disease in the asymptomatic population.

References

1. White HD, Norris RM, Brown MA, Brandt PW, Whitlock RM, Wild CJ. Left ventricular end-systolic volume as the major determinant of survival after recovery from myocardial infarction. Circulation. 1987 Jul;76(1):44-51. doi: 10.1161/01.cir.76.1.44. PMID: 3594774.

2. Di Donato M, Dabic P, Castelvecchio S, Santambrogio C, Brankovic J, Collarini L, Joussef T, Frigiola A, Buckberg G, Menicanti L; RESTORE Group. Left ventricular geometry in normal and post-anterior myocardial infarction patients: sphericity index and 'new' conicity index comparisons. Eur J Cardiothorac Surg. 2006 Apr;29 Suppl 1:S225-30. doi: 10.1016/j.ejcts.2006.03.002. Epub 2006 Mar 27. PMID: 16564696.

3. Lieb W, Gona P, Larson MG, Aragam J, Zile MR, Cheng S, Benjamin EJ, Vasan RS. The natural history of left ventricular geometry in the community: clinical correlates and prognostic significance of change in LV geometric pattern. JACC Cardiovasc Imaging. 2014 Sep;7(9):870-8. doi: 10.1016/j.jcmg.2014.05.008. Epub 2014 Aug 13. PMID: 25129518; PMCID: PMC4163746.

4. Velagaleti RS, Gona P, Pencina MJ, Aragam J, Wang TJ, Levy D, D'Agostino RB, Lee DS, Kannel WB, Benjamin EJ, Vasan RS. Left ventricular hypertrophy patterns and incidence of heart failure with preserved versus reduced ejection fraction. Am J Cardiol. 2014 Jan 1;113(1):117-22. doi: 10.1016/j.amjcard.2013.09.028. Epub 2013 Oct 4. PMID: 24210333; PMCID: PMC3881171.

5. Vasan RS, Larson MG, Benjamin EJ, Evans JC, Levy D. Left ventricular dilatation and the risk of congestive heart failure in people without myocardial infarction. N Engl J Med. 1997 May 8;336(19):1350-5. doi: 10.1056/NEJM199705083361903. PMID: 9134875.

6. [6] Lauer MS, Evans JC, Levy D. Prognostic implications of subclinical left ventricular dilatation and systolic dysfunction in men free of overt cardiovascular disease (the Framingham Heart Study). Am J Cardiol. 1992 Nov 1;70(13):1180-4. doi: 10.1016/0002-9149(92)90052-z. PMID: 1414943.

7. Kannel WB, Levy D, Cupples LA. Left ventricular hypertrophy and risk of cardiac failure: insights from the Framingham Study. J Cardiovasc Pharmacol. 1987;10 Suppl 6:S135-40. PMID: 2485019.

8. Bluemke DA, Kronmal RA, Lima JA, Liu K, Olson J, Burke GL, Folsom AR. The relationship of left ventricular mass and geometry to incident cardiovascular events: the MESA (Multi-Ethnic Study of Atherosclerosis) study. J Am Coll Cardiol. 2008 Dec 16;52(25):2148-55. doi: 10.1016/j.jacc.2008.09.014. PMID: 19095132; PMCID: PMC2706368.

9. Ambale-Venkatesh B, Yoneyama K, Sharma RK, Ohyama Y, Wu CO, Burke GL, Shea S, Gomes AS, Young AA, Bluemke DA, Lima JA. Left ventricular shape predicts different types of cardiovascular events in the general population. Heart. 2017 Apr;103(7):499-507. doi: 10.1136/heartjnl-2016-310052. Epub 2016 Sep 30. PMID: 27694110.

10. Medrano-Gracia P, Cowan BR, Ambale-Venkatesh B, Bluemke DA, Eng J, Finn JP, Fonseca CG, Lima JA, Suinesiaputra A, Young AA. Left ventricular shape variation in asymptomatic populations: the Multi-Ethnic Study of Atherosclerosis. J Cardiovasc Magn Reson. 2014 Jul 30;16(1):56. doi: 10.1186/s12968-014-0056-2. PMID: 25160814; PMCID: PMC4145340.

11. Zhang X, Cowan BR, Bluemke DA, Finn JP, Fonseca CG, Kadish AH, Lee DC, Lima JA, Suinesiaputra A, Young AA, Medrano-Gracia P. Atlas-based quantification of cardiac remodeling due to myocardial infarction. PLoS One. 2014 Oct 31;9(10):e110243. doi: 10.1371/journal.pone.0110243. PMID: 25360520; PMCID: PMC4215861.

12. Albà X, Lekadir K, Pereañez M, Medrano-Gracia P, Young AA, Frangi AF. Automatic initialization and quality control of large-scale cardiac MRI segmentations. Med Image Anal. 2018 Jan;43:129-141. doi: 10.1016/j.media.2017.10.001. Epub 2017 Oct 16. PMID: 29073531.

13. Gilbert K, Bai W, Mauger C, Medrano-Gracia P, Suinesiaputra A, Lee AM, Sanghvi MM, Aung N, Piechnik SK, Neubauer S, Petersen SE, Rueckert D, Young AA. Independent Left Ventricular Morphometric Atlases Show Consistent Relationships with Cardiovascular Risk Factors: A UK Biobank Study. Sci Rep. 2019 Feb 4;9(1):1130. doi: 10.1038/s41598-018-37916-6. PMID: 30718635; PMCID: PMC6362245.

14. Ambale-Venkatesh B, Yang X, Wu CO, Liu K, Hundley WG, McClelland R, Gomes AS, Folsom AR, Shea S, Guallar E, Bluemke DA, Lima JAC. Cardiovascular Event Prediction by Machine Learning: The Multi-Ethnic Study of Atherosclerosis. Circ Res. 2017 Oct 13;121(9):1092-1101. doi: 10.1161/CIRCRESAHA.117.311312. Epub 2017 Aug 9. PMID: 28794054; PMCID: PMC5640485.

15. Bild DE, Bluemke DA, Burke GL, Detrano R, Diez Roux AV, Folsom AR, Greenland P, Jacob DR Jr, Kronmal R, Liu K, Nelson JC, O'Leary D, Saad MF, Shea S, Szklo M, Tracy RP. Multi-Ethnic Study of Atherosclerosis: objectives and design. Am J Epidemiol. 2002 Nov 1;156(9):871-81. doi: 10.1093/aje/kwf113. PMID: 12397006.

16. Suinesiaputra A, Mauger CA, Ambale-Venkatesh B, Bluemke DA, Dam Gade J, Gilbert K, Janse MHA, Hald LS, Werkhoven C, Wu CO, Lima JAC, Young AA. Deep Learning Analysis of Cardiac MRI in Legacy Datasets: Multi-Ethnic Study of Atherosclerosis. Front Cardiovasc Med. 2022 Jan 21;8:807728. doi: 10.3389/fcvm.2021.807728. PMID: 35127868; PMCID: PMC8813768.

17. Natori S, Lai S, Finn JP, Gomes AS, Hundley WG, Jerosch-Herold M, Pearson G, Sinha S, Arai A, Lima JA, Bluemke DA. Cardiovascular function in multi-ethnic study of atherosclerosis: normal values by age, sex, and ethnicity. AJR Am J Roentgenol. 2006 Jun;186(6 Suppl 2):S357-65. doi: 10.2214/AJR.04.1868. PMID: 16714609.

18. Geladi, Paul, and Bruce R. Kowalski. "Partial least-squares regression: a tutorial." *Analytica chimica acta* 185 (1986): 1-17.

19. Ishwaran, Hemant, et al. "Random survival forests." *The annals of applied statistics* 2.3 (2008): 841-860.

20. Kronmal, Richard A. "Spurious correlation and the fallacy of the ratio standard revisited." *Journal of the Royal Statistical Society: Series A (Statistics in Society)* 156.3 (1993): 379-392.

21. Team, R. Core. "R: A language and environment for statistical computing." (2013): 201.

22. Kattan MW, Gerds TA. The index of prediction accuracy: an intuitive measure useful for evaluating risk prediction models. Diagn Progn Res. 2018 May 4;2:7. doi: 10.1186/s41512-018-0029-2. PMID: 31093557; PMCID: PMC6460739.

23. Blanche, Paul, Aurélien Latouche, and Vivian Viallon. "Time-dependent AUC with right-censored data: a survey." *Risk assessment and evaluation of predictions*. Springer, New York, NY, 2013. 239-251.

24. Tsao CW, Gona PN, Salton CJ, Chuang ML, Levy D, Manning WJ, O'Donnell CJ. Left Ventricular Structure and Risk of Cardiovascular Events: A Framingham Heart Study Cardiac Magnetic Resonance Study. J Am Heart Assoc. 2015 Sep 15;4(9):e002188. doi: 10.1161/JAHA.115.002188. PMID: 26374295; PMCID: PMC4599505.

25. Zile MR, Gaasch WH, Patel K, Aban IB, Ahmed A. Adverse left ventricular remodeling in community-dwelling older adults predicts incident heart failure and mortality. JACC Heart Fail. 2014 Oct;2(5):512-22. doi: 10.1016/j.jchf.2014.03.016. Epub 2014 Sep 3. Erratum in: JACC Heart Fail. 2014 Dec;2(6):678. PMID: 25194295.

26. Aung N, Vargas JD, Yang C, Cabrera CP, Warren HR, Fung K, Tzanis E, Barnes MR, Rotter JI, Taylor KD, Manichaikul AW, Lima JAC, Bluemke DA, Piechnik SK, Neubauer S, Munroe PB, Petersen SE. Genome-Wide Analysis of Left Ventricular Image-Derived Phenotypes Identifies Fourteen Loci Associated With Cardiac Morphogenesis and Heart Failure Development. Circulation. 2019 Oct 15;140(16):1318-1330. doi: 10.1161/CIRCULATIONAHA.119.041161. Epub 2019 Sep 25. PMID: 31554410; PMCID: PMC6791514.

27. Davis J, Davis LC, Correll RN, Makarewich CA, Schwanekamp JA, Moussavi-Harami F, Wang D, York AJ, Wu H, Houser SR, Seidman CE, Seidman JG, Regnier M, Metzger JM, Wu JC, Molkentin JD. A Tension-Based Model Distinguishes Hypertrophic versus Dilated Cardiomyopathy. Cell. 2016 May 19;165(5):1147-1159. doi: 10.1016/j.cell.2016.04.002. Epub 2016 Apr 21. PMID: 27114035; PMCID: PMC4874838.

28. Tadros R, Francis C, Xu X, Vermeer AMC, Harper AR, Huurman R, Kelu Bisabu K, Walsh R, Hoorntje ET, Te Rijdt WP, Buchan RJ, van Velzen HG, van Slegtenhorst MA, Vermeulen JM, Offerhaus JA, Bai W, de Marvao A, Lahrouchi N, Beekman L, Karper JC, Veldink JH, Kayvanpour E, Pantazis A, Baksi AJ, Whiffin N, Mazzarotto F, Sloane G, Suzuki H, Schneider-Luftman D, Elliott P, Richard P, Ader F, Villard E, Lichtner P, Meitinger T, Tanck MWT, van Tintelen JP, Thain A, McCarty D, Hegele RA, Roberts JD, Amyot J, Dubé MP, Cadrin-Tourigny J, Giraldeau G, L'Allier PL, Garceau P, Tardif JC, Boekholdt SM, Lumbers RT, Asselbergs FW, Barton PJR, Cook SA, Prasad SK, O'Regan DP, van der Velden J, Verweij KJH, Talajic M, Lettre G, Pinto YM, Meder B, Charron P, de Boer RA, Christiaans I, Michels M, Wilde AAM, Watkins H, Matthews PM, Ware JS, Bezzina CR. Shared genetic pathways contribute to risk of hypertrophic and dilated cardiomyopathies with opposite directions of effect. Nat Genet. 2021 Feb;53(2):128-134. doi: 10.1038/s41588-020-00762-2. Epub 2021 Jan 25. PMID: 33495596; PMCID: PMC7611259.

29. Morris DA, Ma XX, Belyavskiy E, Aravind Kumar R, Kropf M, Kraft R, Frydas A, Osmanoglou E, Marquez E, Donal E, Edelmann F, Tschöpe C, Pieske B, Pieske-Kraigher E. Left ventricular longitudinal systolic function analysed by 2D speckle-tracking echocardiography in heart failure with preserved ejection fraction: a meta-analysis. Open Heart. 2017 Sep 25;4(2):e000630. doi: 10.1136/openhrt-2017-000630. PMID: 29018535; PMCID: PMC5623331.

30. Szelényi Z, Fazakas Á, Szénási G, Tegze N, Fekete B, Molvarec A, Hadusfalvy-Sudár S, Jánosi O, Kiss M, Karádi I, Vereckei A. The mechanism of reduced longitudinal left ventricular systolic function in hypertensive patients with normal ejection fraction. J Hypertens. 2015 Sep;33(9):1962-9; discussion 1969. doi: 10.1097/HJH.0000000000000624. PMID: 26154942.

31. Ahmed MI, Desai RV, Gaddam KK, Venkatesh BA, Agarwal S, Inusah S, Lloyd SG, Denney TS Jr, Calhoun D, Dell'italia LJ, Gupta H. Relation of torsion and myocardial strains to LV ejection fraction in hypertension. JACC Cardiovasc Imaging. 2012 Mar;5(3):273-81. doi: 10.1016/j.jcmg.2011.11.013. PMID: 22421172; PMCID: PMC3321569.

32. Heinzel FR, Hohendanner F, Jin G, Sedej S, Edelmann F. Myocardial hypertrophy and its role in heart failure with preserved ejection fraction. J Appl Physiol (1985). 2015 Nov 15;119(10):1233-42. doi: 10.1152/japplphysiol.00374.2015. Epub 2015 Jul 16. PMID: 26183480; PMCID: PMC4652334

33. Ahmed MI, Desai RV, Gaddam KK, Venkatesh BA, Agarwal S, Inusah S, Lloyd SG, Denney TS Jr, Calhoun D, Dell'italia LJ, Gupta H. Relation of torsion and myocardial strains to LV ejection fraction in hypertension. JACC Cardiovasc Imaging. 2012 Mar;5(3):273-81. doi: 10.1016/j.jcmg.2011.11.013. PMID: 22421172; PMCID: PMC3321569.

34. Ng AC, Delgado V, Bertini M, van der Meer RW, Rijzewijk LJ, Shanks M, Nucifora G, Smit JW, Diamant M, Romijn JA, de Roos A, Leung DY, Lamb HJ, Bax JJ. Findings from left ventricular strain and strain rate imaging in asymptomatic patients with type 2 diabetes mellitus. Am J Cardiol. 2009 Nov 15;104(10):1398-401. doi: 10.1016/j.amjcard.2009.06.063. Epub 2009 Sep 26. PMID: 19892057.

35. Pavlopoulos H, Grapsa J, Stefanadi E, Philippou E, Dawson D, Nihoyannopoulos P. Is it only diastolic dysfunction? Segmental relaxation patterns and longitudinal systolic

deformation in systemic hypertension. Eur J Echocardiogr. 2008 Nov;9(6):741-7. doi: 10.1093/ejechocard/jen133. Epub 2008 Apr 4. PMID: 18490299.

36. Medrano-Gracia P, Cowan BR, Bluemke DA, Finn JP, Kadish AH, Lee DC, Lima JA, Suinesiaputra A, Young AA. Atlas-based analysis of cardiac shape and function: correction of regional shape bias due to imaging protocol for population studies. J Cardiovasc Magn Reson. 2013 Sep 13;15(1):80. doi: 10.1186/1532-429X-15-80. PMID: 24033990; PMCID: PMC3848808.

37. Izquierdo C, Casas G, Martin-Isla C, Campello VM, Guala A, Gkontra P, Rodríguez-Palomares JF, Lekadir K. Radiomics-Based Classification of Left Ventricular Non-compaction, Hypertrophic Cardiomyopathy, and Dilated Cardiomyopathy in Cardiovascular Magnetic Resonance. Front Cardiovasc Med. 2021 Oct 29;8:764312. doi: 10.3389/fcvm.2021.764312. PMID: 34778415; PMCID: PMC8586199.

38. Rauseo E, Izquierdo Morcillo C, Raisi-Estabragh Z, Gkontra P, Aung N, Lekadir K, Petersen SE. New Imaging Signatures of Cardiac Alterations in Ischaemic Heart Disease and Cerebrovascular Disease Using CMR Radiomics. Front Cardiovasc Med. 2021 Sep 23;8:716577. doi: 10.3389/fcvm.2021.716577. PMID: 34631820; PMCID: PMC8494975.

39. Suinesiaputra A, Ablin P, Alba X, Alessandrini M, Allen J, Bai W, Cimen S, Claes P, Cowan BR, D'hooge J, Duchateau N, Ehrhardt J, Frangi AF, Gooya A, Grau V, Lekadir K, Lu A, Mukhopadhyay A, Oksuz I, Parajali N, Pennec X, Pereanez M, Pinto C, Piras P, Rohe MM, Rueckert D, Saring D, Sermesant M, Siddiqi K, Tabassian M, Teresi L, Tsaftaris SA, Wilms M, Young AA, Zhang X, Medrano-Gracia P. Statistical shape modeling of the left ventricle: myocardial infarct classification challenge. IEEE J Biomed

Health Inform. 2018 Mar;22(2):503-515. doi: 10.1109/JBHI.2017.2652449. Epub 2017 Jan 17. PMID: 28103561; PMCID: PMC5857476.

Tables

Table 1: Cohort statistics at baseline

	Event-free population (n=4,097)	*HF (n=147)*	*CHD (n=317)*	*CVD (n=455)*
Age (years)	60.6±9.9	68.7±8.4*	66.1±9.3*	66.6±9.3*
Gender (% Male)	45	66.6*	70*	63*
Height (cm)	166±9.9	168.7±10.6	168.4±9.7	167.3±10
Weight (kg)	76.7±15.9	81.2±16*	79.8±15.8*	79.4±15.5*
LVMi (g/m2)	76.9±15.1	95.2±24.2*	84.8±19.2*	85±19.7*
LV EF (%)	69.1±7.0	64.2±11.5*	68.3±8.4*	68.3±8.5*
EDVi (ml/m2)	68.1±12.9	75.9±21.4*	67.9±15.6	67.7±15.8
ESVi (ml/m2)	21.2±7.3	28.7±17.4*	22.1±10.1	22.1±10.8
NT-proBNP (pg/mg)	81.7±132	406±1,148*	203.1±777.2*	204±683*
Smokers (%)	11.9	17*	17*	18*
CACS (%)	43.9	73.4*	82.6*	80.2*
SBP (mmHg)	125.4±20.6	136.9±22.5*	133.9±22.4*	135.2±22.8*
HTN medication (%)	32	55.7*	50*	50*
Diabetes (%)	8	24.4*	19.8*	19*
HDL (mg/dL)	51.6±15	48.7±14.2*	47±13.7*	47.7±13.5*
Total cholesterol (mg/dL)	169±25.9	188.6±35.2*	193.1±37.2*	192±36*
Heart Rate (bpm)	62.2±9.2	65.5±10.9*	63.8±10.6*	63.8±10.3*
Beta-blocker use (%)	8	12.2*	33*	47*

Continuous variables are expressed as mean ± standard deviation and were compared using a Student's t-test or Welch's t-test depending on the population's variance. Categorical variables are expressed as frequency and were compared using a Pearson's chi-squared test. * symbol indicates $p < 0.05$ event-free after 10 years population vs event populations. Note that one participant could be associated to multiple outcomes. ***Abbreviations:*** CACS: Coronary calcium score, CHD: coronary heart disease, CVD: cardiovascular disease, HF: heart failure, HTN medication: hypertensive medication use, NT-proBNP: N-terminal pro-brain natriuretic peptide, SBP: systolic blood pressure.

Table 2: Average models performance and calibration for 10-year survival across the five folds for incident HF, CHD and CVD.

Outcome	*Performance measure*	*M1*	*M2*	*M3*
HF	IPA (%)	7.9±1.7	11.9±2.8	14.6±2.4
	AUC at 10-y	0.80±0.02	0.81±0.01	0.83±0.01*
	Sensitivity at 10-y	0.76±0.01	0.78±0.02	0.80±0.02
	PPV at 10-y	9.2±0.06	12.0±0.07	13.7±0.04
CVD	IPA (%)	11.7±1.3	11.8±1.3	12.7±1.2
	AUC at 10-y	0.76±0.01	0.76±0.01	0.78±0.00*
	Sensitivity at 10-y	0.70±0.01	0.72±0.01	0.74±0.01
	PPV at 10-y	20.4±0.07	20±0.06	22.5±0.1
CHD	IPA (%)	10.6±0.5	11.0±0.2	11.5±0.8
	AUC at 10-y	0.75±0.02	0.75±0.01	0.77±0.01*
	Sensitivity at 10-y	0.73±0.01	0.72±0.02	0.77±0.01
	PPV at 10-y	16.3±0.01	17.9±0.01	18.6±0.2

Values are mean ± standard deviation. * AUC $p<0.05$ between M2 and M3 (no tests for IPA, Sensitivity or PPV).

PPV was used instead of specificity as we are dealing with rare events.

M1: age, sex, race, body mass index, height, weight, smoking, systolic blood pressure, use of anti-hypertensive medications, diabetes mellitus, fasting glucose, high-density lipoprotein, total cholesterol, resting heart rate, and beta-blocker.

M2: M1 + ejection fraction, left ventricular (LV) mass, LV end systolic and end diastolic volumes.

M3: M1 + 30 event-specific remodeling signatures derived from the PLS analysis

Abbreviations: AUC: area under the receiver operating characteristics curve, CHD: coronary heart disease, CVD: cardiovascular disease, HF: heart failure, IPA: index of prediction accuracy, PPV: positive predictive value.

Table 3: Top ranked variables based on the mean of the minimal depth of the maximal subtree over the entire forest.

HF	CVD	CHD
RS1	CACS	CACS
NT-proBNP	Age	SBP
RS2	RS1	Smoking
RS3	SBP	RS1
Age	RS2	RS2
Fasting glucose	RS3	Age

Abbreviations: HF: heart failure, CACS: Coronary calcium score, CHD: coronary heart disease, CVD: cardiovascular disease, NT-proBNP: N-terminal pro-brain natriuretic peptide. RS: remodeling signatures. SBP: systolic blood pressure.

Table S1: Hazard ratios and 95% confidence intervals for the selected variables for each outcome. SBP: systolic blood pressure. HDL: high density lipoprotein. RS: remodeling signature.

CHF	
Selected variables	*Hazard ratios [95% confidence intervals]*
NT-proBNP	1.70 [1.34,2.15]
Age	1.07 [1.05,1.10]
Fasting glucose	1.03 [1.01,1.06]
Resting Heart Rate	1.01 [1.01,1.02]
RS1	0.55 [0.47,0.63]
RS2	0.66 [0.54,0.83]
RS3	0.72 [0.59,0.89]
SBP	0.98 [0.80,1.20]

CHD	
Selected variables	*Hazard ratios [95% confidence intervals]*
Calcium score	2.24 [1.90,2.64]
SBP	1.14 [0.96,1.37]
Age	1.02 [1.10,1.38]
RS1	0.79 [0.69,0.92]
RS2	0.80 [0.70,0.92]
HDL level	0.90 [0.77,1.01]
Smoking	1.11 [0.98,1.27]

CVD	
Selected variables	*Hazard ratios [95% confidence intervals]*
Calcium score	1.78 [1.56,2.03]
RS1	0.74 [0.66,0.83]
SBP	1.18 [1.06,1.32]
Age	1.29 [1.10,1.50]
RS2	0.81 [0.71,0.90]
HDL level	0.83 [0.72,0.95]
RS4	0.83 [0.74,0.92]
RS5	0.85 [0.77,0.95]
RS3	0.82 [0.73,0.92]
Fasting glucose	1.11 [1.02,1.20]
RS6	0.85 [0.76,0.95]
RS7	0.87 [0.78,0.97]
RS8	0.87 [0.80,1.01]
Heart rate	1.10 [1.02,1.21]
RS9	0.84 [0.74,0.95]

Figure Legends

Figure 1 - Flow diagram of data inclusion. MESA = Multi-Ethnic Study of Atherosclerosis.

Figure 2 - Correlation coefficients between the top remodeling signatures for each endpoint - Each ellipse approximates the shape of a bivariate normal distribution with the same correlation. Colors represent the strength and direction of the correlation. Correlation coefficients were multiplied by -1 for better visualization and interpretation, as time-to-event was used for the regression meaning that a decrease in z-score was associated with an increase in probability of event. EDVi: indexed end-diastolic volume, ESVi: indexed end-systolic volume. LVMi: indexed LV mass. RS: remodeling signatures. Only significant values ($p<0.05$) are reported.

Figure 3 - Top PLS remodeling signatures for incident HF (a), CHD (b) and CVD (c). Top: Remodeling signatures for incident HF (a), CHD (b) and CVD (c) - The mesh on the left shows what a shape in the high-risk category looks like (see bottom row) while the mesh on the right shows what a shape in the low-risk category looks like. ED is shown as wireframe, ES as colored surface. Green: endocardium, red: epicardium. Middle: Kaplan-Meier survival curves of the 2 subgroups (high-risk (blue) and low-risk (yellow)) based on patient-specific z-score, demonstrating prognostic relevance of each remodeling signature. Optimal cut-off for PLS-derived RS separating the two risk groups (high risk vs low risk) was determined using classification and regression trees. Individuals were free of event at baseline. Bottom: Partial dependence plot. Partial values are in red, Loess curve is in dashed black and the error bars of +/- two standard errors are shown in dashed red. The vertical dashed line shows the threshold determined using classification and regression trees separating high-risk vs low-risk groups for each RS.

Figure 4 – Summary of each remodeling signature (RS) in terms of currently understood remodeling patterns. *Top panel*: remodeling signatures associated with heart failure. a) RS1 associated with eccentric hypertrophy; b) RS2 associated with concentric hypertrophy; c) RS3 associated with apical dilation. *Middle panel*: remodeling signatures associated with coronary heart disease. RS1 associated with concentric hypertrophy); b) RS2 associated with eccentric hypertrophy. *Bottom panel:* remodeling signatures associated with cardiovascular disease. RS1 associated concentric hypertrophy; b) RS2 associated with eccentric hypertrophy; c) RS3 associated with sphericity and apical dilation. ***Abbreviations:*** EDVi: indexed end-diastolic volume, ESVi: indexed end-systolic volume, LVMi: indexed left ventricular mass, M:V: mass-to-volume ratio EF: ejection fraction, LS: longitudinal shortening.

Figure S1 - Overview of the processing pipeline. Left panel: Generation of landmarks (mitral valve and right ventricular insertion) and epicardial and endocardial contours using deep neural network methods. Middle panel: contour and landmark points in 3D and correction of breath-hold misregistration between slices. Right panel: model surfaces fitted to contours and landmarks.

Figure S2 - Calculation of clinical indices. Volumes were calculated by numerical integration. LVM was calculated by subtracting endocardial from epicardial volumes, multiplied by 1.05 g/ml. Panel a) Apical conicity (AC) calculation $AC = \frac{d_2}{d_1}$. Panel b) Sphericity (Sph) calculation: $Sph = \frac{chamber\ volume}{\frac{4}{3}\pi r^3}$. Panel c): Relative wall thickness (RWT) calculation: $RWT = 2 \times \frac{R}{d_2}$

Figure S3 - Partial dependence plot of the 3 predictors among cardiovascular risk factors for each event: Top: congestive heart failure, middle: all cardiovascular disease,

bottom: coronary heart disease. Partial values are in red, Loess curve is in dashed black and the error bars of +/- two standard errors are shown in dashed red. HU: Hounsfield units, SBP: systolic blood pressure, NT-proBNP: N-terminal pro-brain natriuretic peptide.

Figure S4 - Correlation between fractional thickening and the first remodeling signature for incident CHF (left) and incident CHD (right) within each of the 17 American Heart Association segments. The 17th segment was excluded.

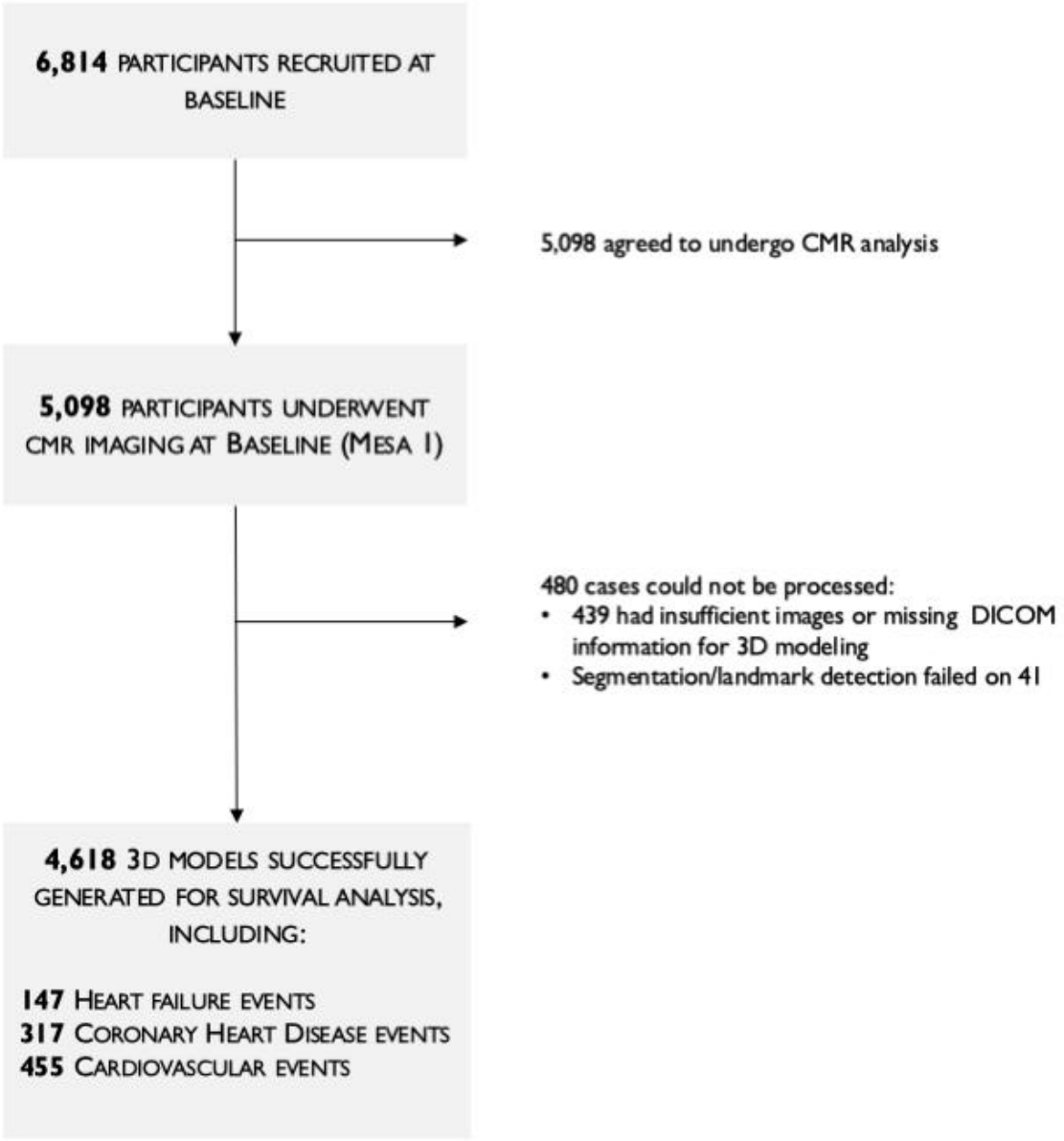

Figure 1 - Flow diagram of participant inclusion. MESA = Multi-Ethnic Study of Atherosclerosis.

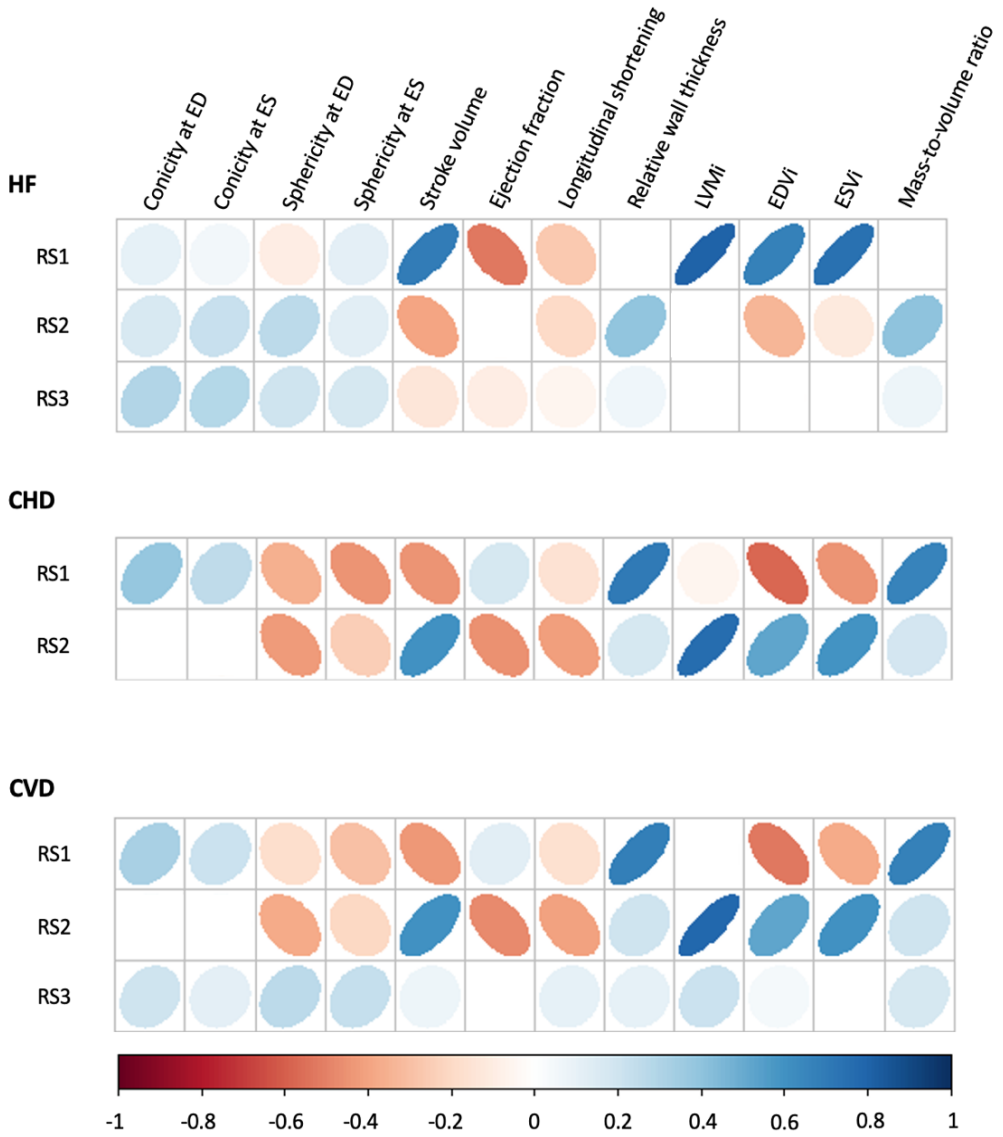

Figure 2 Correlation matrix heatmap shows the correlation coefficients between the top remodeling signatures for heart failure (HF), coronary heart disease (CHD), and cardiovascular disease (CVD) events. Each ellipse approximates the shape of a bivariate normal distribution with the same correlation. Colors represent the strength and direction of the correlation. Correlation coefficients were multiplied by negative one for better visualization and interpreta- tion because the time to event was used for the regression (ie, a decrease in z score was associated with an increase in probability of event). Only significant values ($P < .05$) are reported. ED = end diastole, EDVi = indexed end-diastolic volume, ES = end systole, ESVi = indexed end-systolic volume, LVMi = in- dexed left ventricular mass, RS = remodeling signature.

A

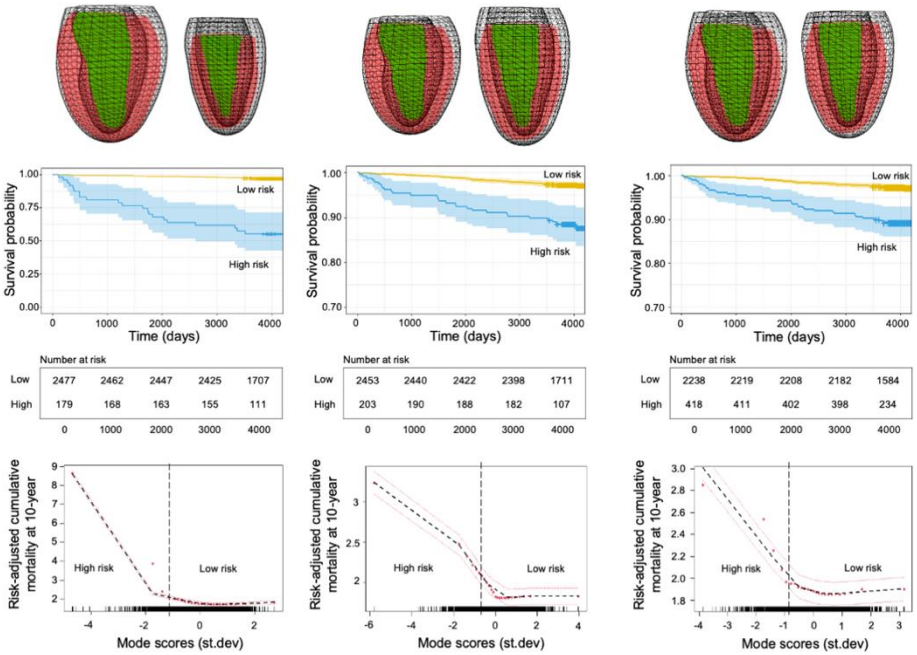
Survival probability
Low risk
High risk
Time (days)
Number at risk
Low 2477 2462 2447 2425 1707
High 179 168 163 155 111
0 1000 2000 3000 4000
Low 2453 2440 2422 2398 1711
High 203 190 188 182 107
Low 2238 2219 2208 2182 1584
High 418 411 402 398 234
Risk-adjusted cumulative mortality at 10-year
Mode scores (st.dev)

B

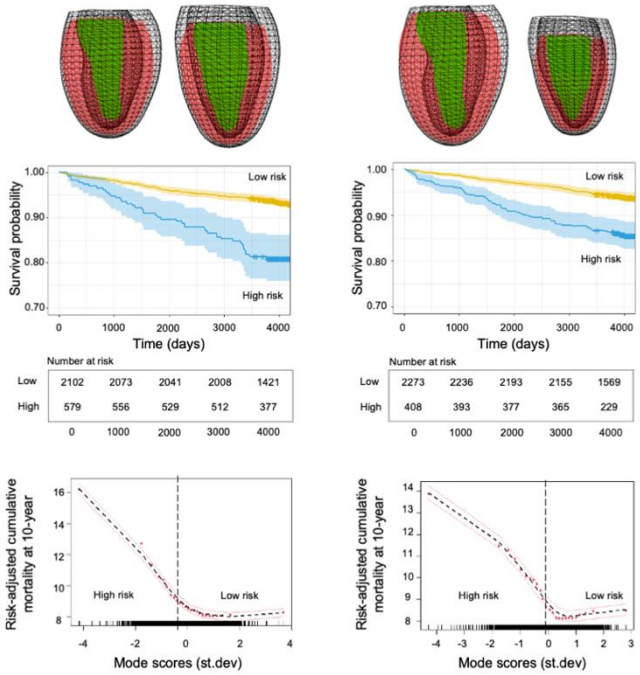
Survival probability
Low risk
High risk
Time (days)
Number at risk
Low 2102 2073 2041 2008 1421
High 579 556 529 512 377
Low 2273 2236 2193 2155 1569
High 408 393 377 365 229
Risk-adjusted cumulative mortality at 10-year
Mode scores (st.dev)

C

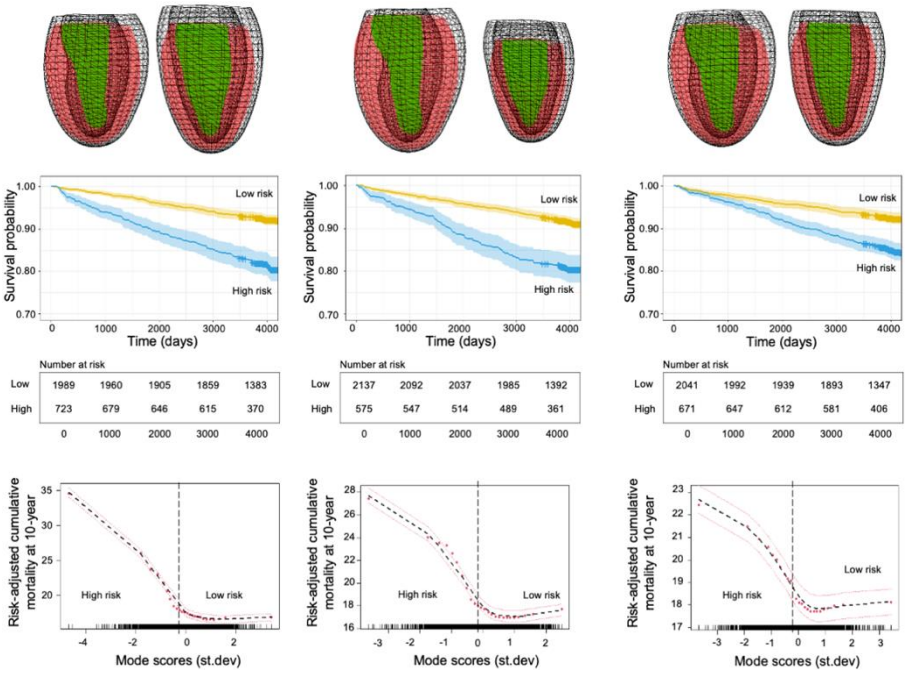

Figure 3 - Top PLS remodeling signatures for incident HF (a), CHD (b) and CVD (c).
Top: The mesh on the left shows what a shape in the high-risk category looks like (see bottom row) while the mesh on the right shows what a shape in the low-risk category looks like. ED is shown as a wireframe, ES as a colored surface. Green: endocardium, red: epicardium.
Middle: Kaplan-Meier survival curves of the 2 subgroups (high-risk (blue) and low-risk (yellow)) based on patient-specific z-score, demonstrating prognostic relevance of each remodeling signature. Optimal cut-off for PLS-derived RS separating the two risk groups (high risk vs low risk) was determined using classification and regression trees. Individuals were free of events at baseline.
Bottom: Partial dependence plot. Partial values are in red, Loess curve is in dashed black and the error bars of +/- two standard errors are shown in dashed red. The vertical dashed line shows the threshold determined using classification and regression trees separating high-risk vs low-risk groups for each RS.

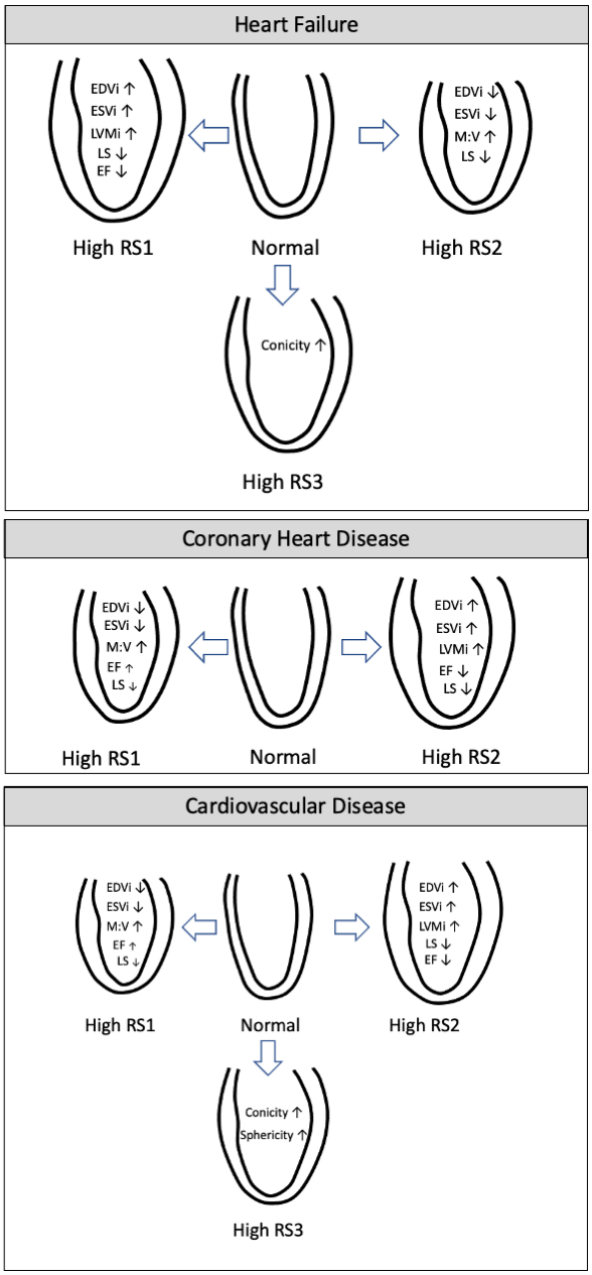

Figure 4 – Summary of each remodeling signature (RS) in terms of currently understood remodeling patterns. *Top panel*: remodeling signatures associated with heart failure. a) RS1 associated with eccentric hypertrophy; b) RS2 associated with concentric hypertrophy; c) RS3 associated with apical dilation. *Middle panel*: remodeling signatures associated with coronary heart disease. RS1 associated with concentric hypertrophy; b) RS2 associated with eccentric hypertrophy. *Bottom panel:* remodeling signatures associated with cardiovascular disease. RS1 associated concentric hypertrophy; b) RS2 associated with eccentric hypertrophy; c) RS3 associated with sphericity and apical dilation. ***Abbreviations:*** EDVi: indexed end-diastolic volume, ESVi: indexed end-systolic volume, LVMi: indexed left ventricular mass, M:V: mass-to-volume ratio EF: ejection fraction, LS: longitudinal shortening

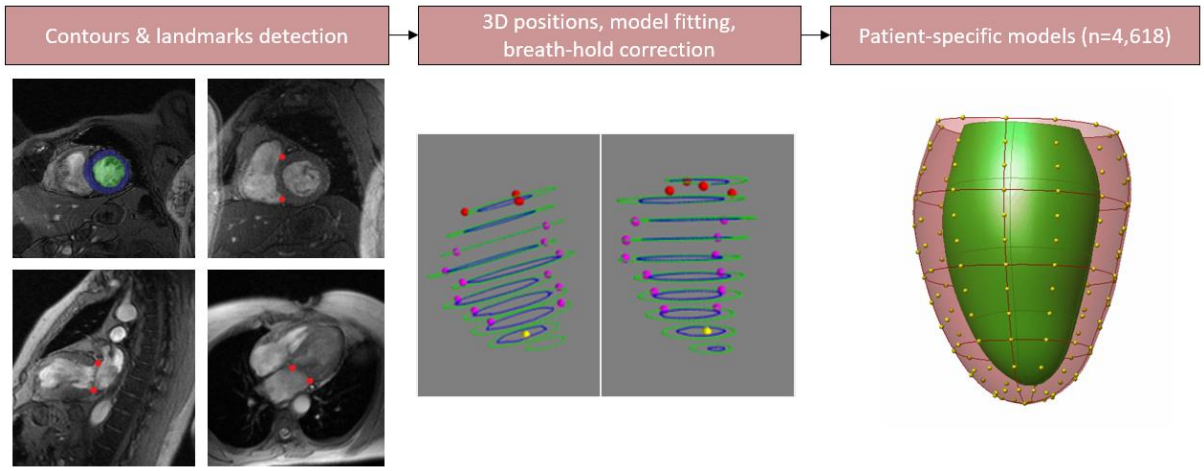

Figure S1 - Overview of the processing pipeline - Left panel: Generation of landmarks (mitral valve and right ventricular insertion) and epicardial and endocardial contours using deep neural network methods. Middle panel: contour and landmark points in 3D and correction of breath-hold misregistration between slices. Right panel: model surfaces fitted to contours and landmarks.

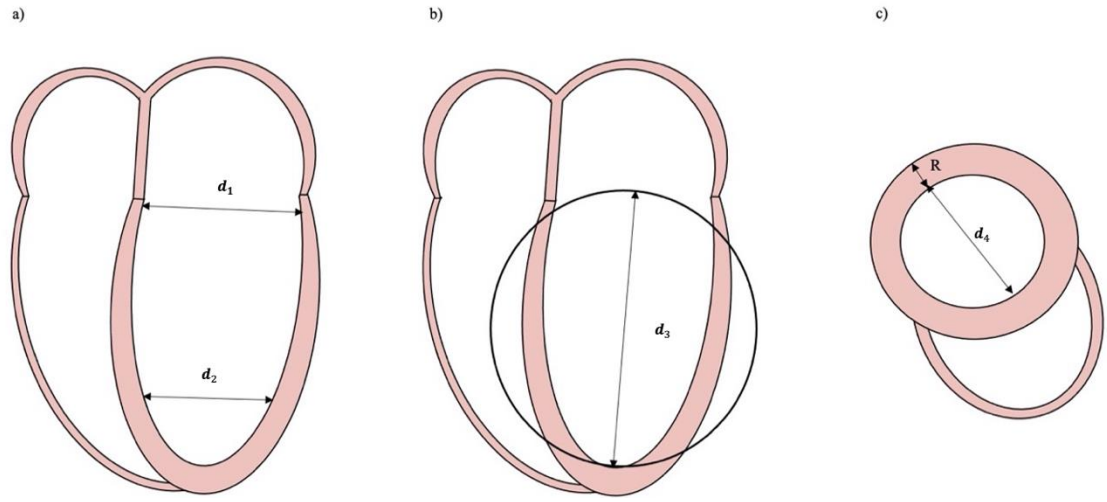

Figure S2 - Calculation of clinical indices. Volumes were calculated by numerical integration. LVM was calculated by subtracting endocardial from epicardial volumes, multiplied by 1.05 g/ml. Panel a) Apical conicity (AC) calculation $AC = \frac{d_2}{d_1}$. Panel b) Sphericity (Sph) calculation: $Sph = \frac{chamber\ volume}{\frac{4}{3}\pi(\frac{d_3}{2})^3}$. Panel c): Relative wall thickness (RWT) calculation: $RWT = 2 \times \frac{R}{d_4}$

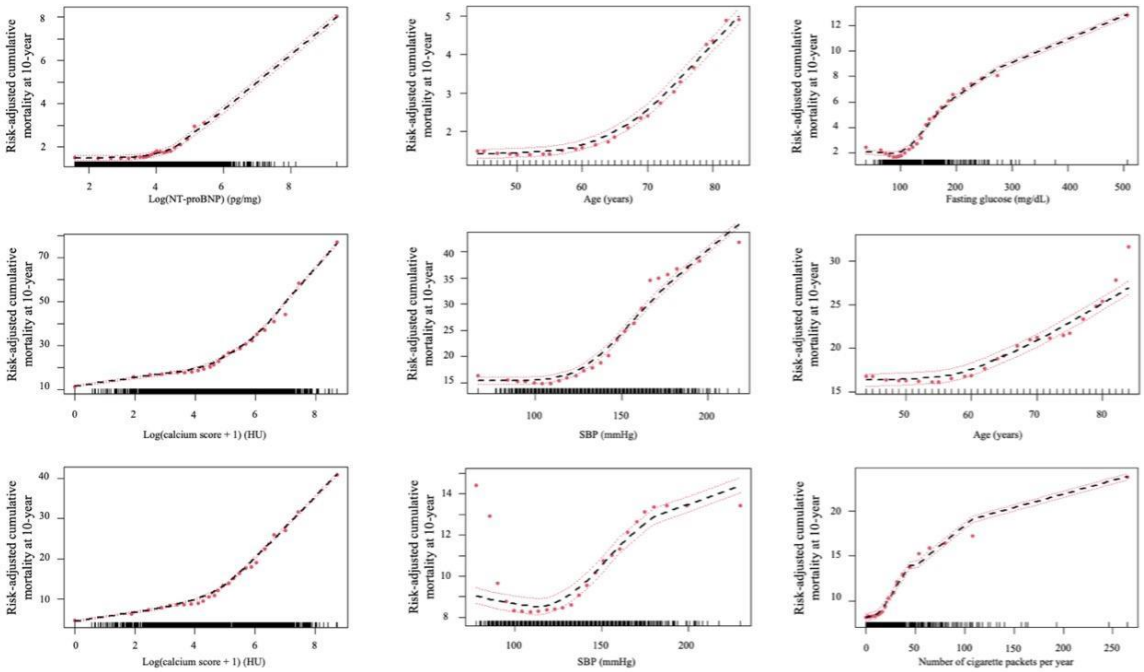

Figure S3 - Partial dependence plot of the 3 predictors among cardiovascular risk factors for each event: Top: congestive heart failure, middle: all cardiovascular disease, bottom: coronary heart disease. Partial values are in red, Loess curve is in dashed black and the error bars of +/- two standard errors are shown in dashed red. HU: Hounsfield units, SBP: systolic blood pressure, NT-proBNP: N-terminal pro-brain natriuretic peptide.

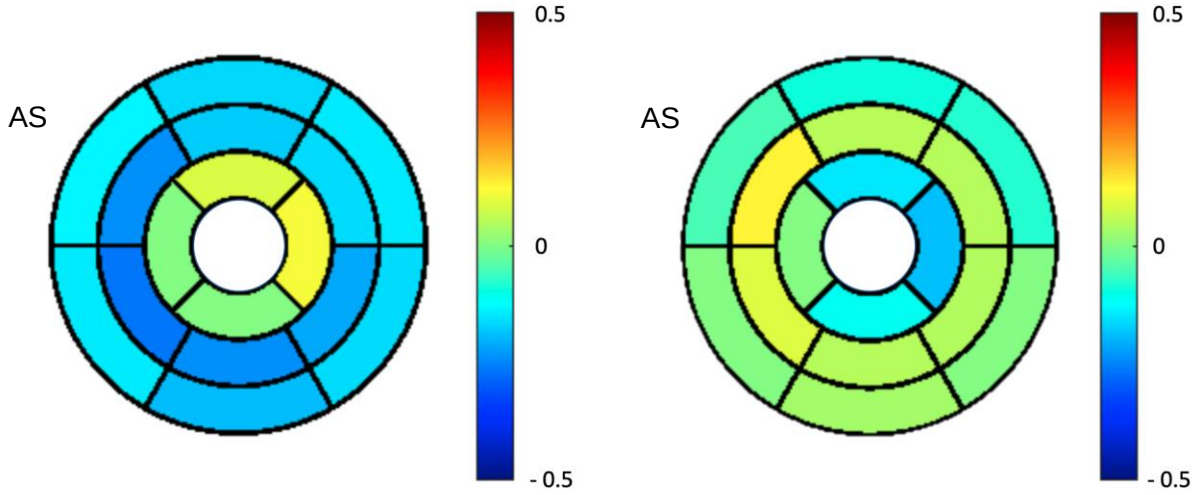

Figure S4 - Correlation between fractional thickening and the first remodeling signature for incident HF (left) and incident CHD (right) within each of the 17 American Heart Association segments. The 17th segment was excluded. AS: antero-septal region.